Methyl Chloride ν_5 Region Line Shape Parameters and Rotational Constants for the ν_2, ν_5 and $2\nu_3$ Vibrational Bands

by

C. Chackerian, Jr.*

NASA Ames Research Center, Moffett Field, CA 94035

L. R. Brown

Jet Propulsion Laboratory, California Institute of Technology, Oak Grove Drive, Pasadena, CA 91109

N. Lacome

Laboratoire de Spectrochimie Moléculaire, URA CNRS 508, Université Pierre et Marie Curie (Paris 6), Bâtiment F 74, 4 Place Jussieu, 75252 Paris Cedex 05, France
LADIR, CNRS UPR A1580
2 rue Henri Dunant, 94320 Thiais, France

G. Tarrago

LPMA, Batiment 350, Universite de Paris XI, 91405 Orsay, France

*Correspondent.

Abstract-Fourier spectra of methyl chloride have been obtained at ambient laboratory temperature under self-broadening conditions. Five-thousand two-hundred and sixty rovibrational transitions of the (ν_2, ν_5 ,$2\nu_3$)-vibrational-band triad have been assigned and new ground and excited state rotational constants for $CH_3{}^{35}Cl$ and $CH_3{}^{37}Cl$ determined. The ν_5 and ν_2 vibrational-band intensities are determined to be respectively 42(1.2) and 31.7(0.9) $cm^{-2}atm^{-1}$. Self-broadening coefficients of individual rovibrational lines are determined for the ν_5 band of $CH_3{}^{35}Cl$ and $CH_3{}^{37}Cl$ at 296 K. The self-broadening coefficients peak broadly close to the maximum in the Boltzmann rotational population; no specific trends of the broadening coefficients are observed with the rotational quantum number K. With the exception of the $^RQ(J,0)$ branch, the 1260 cm^{-1} to 1650 cm^{-1} spectral region can be well modeled by the superposition of overlapping Voigt line profiles. To adequately model the densely-packed $^RQ(J,0)$ branch, however, we included collisional line mixing with A^+ to A^- in addition to A^- to A^- and A^+ to A^+ $|\Delta J| \geq 1$, $\Delta K=0$ collisional transitions allowed.

INTRODUCTION

Methyl chloride (CH_3Cl) is relatively abundant in the Earth's atmosphere, and because it is easily photodissociated is an important source of the chlorine atoms which are involved in the destruction of atmospheric ozone. Elkins *et al.* (1) in their report of infrared band strengths have cited references which discuss the implications of methyl chloride for atmospheric ozone chemistry as well as its' importance as a greenhouse gas.

The strongest feature in the six vibrational fundamental bands of CH_3Cl recorded, at a resolution of 0.04 cm^{-1}, by Elkins *et al.* (1) is the $^RQ(J,0)$ Q branch of the ν_5 band at about 1459.6 cm^{-1}. While ν_5 is not the strongest of the six fundamental vibrational bands, the $^RQ(J,0)$ Q branch of this band is the strongest single spectroscopic feature because collisional line mixing narrows and sharpens some 120 nearly superimposed lines

from both the $CH_3{}^{35}Cl$ and $CH_3{}^{37}Cl$ isotopic species. With the idea that this feature can be used for monitoring CH_3Cl in the earth's atmosphere via infrared techniques, we have determined many of the relevant spectroscopic parameters necessary for interpreting field measurements. Infrared spectroscopic experiments which monitor CH_3Cl in the atmosphere require line shape information under N_2- and O_2-broadening conditions. So in addition to the pure gas spectra analyzed for this paper, we have also recorded low-temperature spectra of methyl chloride spectra recorded under nitrogen-broadening conditions. These spectra have not been analyzed but low-temperature broadening by nitrogen in the ν_3 band of CH_3Cl have been previously reported (2, 3). Since CH_3Cl has such large self-broadening coefficients any laboratory data on the CH_3Cl-N_2, or CH_3Cl-O_2 systems needs to be corrected for self-collisional effects. Since the initiation of this work other papers have appeared on the shape of the $^RQ(J,0)$ Q branch of CH_3Cl when it is perturbed by helium (4) as well as nitrogen (5). These latter studies involve a simple but practical technique for semi-empirically modeling the line mixing in CH_3Cl. Our work emphasizes a somewhat more detailed mechanistic approach to the line mixing, albeit for self broadening.

Since we could not spectroscopically resolve individual rovibrational transitions of the $^RQ(J,0)$ Q branch up to $J'' = 36$, we have had to deduce those relevant line positions, intensities and broadening coefficients from measurements and modeling of a large number of transitions found outside of this Q branch. Because of the importance of Fermi and Coriolis resonances it was necessary to model simultaneously the ν_2, ν_5, and $2\nu_3$ vibrational bands. The extensive measurements, analysis and calculation of

these line parameters as well as modeling of the absorption profile of ν_5 band $^{R}Q(J,0)$ branch are the subjects of this paper.

EXPERIMENTAL DETAILS

The methyl chloride spectra were recorded with the Fourier transform spectrometer (FTS) at the McMath Solar Telescope located at the Kitt Peak National Observatory/National Solar Observatory using helium-cooled Arsenic-doped Silicon detectors, CaF_2 beamsplitters and a globar source. Each spectrum was integrated for one hour to achieve signal to noise ratios of 300:1 or better at 0.0056 cm^{-1} resolution in the 1000 to 2900 cm^{-1} bandpass. The interferograms were weakly apodized as described in our previous paper (6) [see Eq. 1]; in practice the instrumental resolution was degraded by about 10% because of the divergence of the infrared beam due to the finite diameter of the entrance aperture. All spectra were recorded at room temperature at the gas conditions shown in Table 1. The gas sample, with chlorine in natural abundance (nominally 75.5% ^{35}Cl and 24.5% ^{37}Cl), was obtained from Matheson, and gas pressures were measured continually with Baratron capacitance manometers. Temperatures were measured by thermisters in thermal contact with the exterior of the absorption cells.

Spectral features arising from residual water inside the FTS vacuum chamber were used to calibrate the wavenumber scale of these data (7). Line centers determined primarily from the fourth spectrum in Table 1 were retrieved via peak finding, while the self-broadened widths and intensities were measured using non-linear least-squares curve-fitting techniques (8). Since the primary objective of the analysis was the study of

line shapes in the $^{R}Q(J,0)$ branch, only a limited number of line intensities were obtained. The self-broadening coefficients we measured are presented graphically and a limited number are tabulated.

Table 2 gives a sample of the measurements for $^{R}R(J,0)$ transitions, giving by lower state J" the observed positions, intensities, and widths (columns 2, 4 and 5, and 7 respectively). Also shown in Table 2 are the differences between the positions and intensities obtained from the low and high pressure data; L and H indicate respectively that the values were retrieved from the first four spectra or the last four spectra in Table 1. The comparisons between the high and low pressure data are thought to provide a valid indication of the experimental precision of these parameters.

ROVIBRATIONAL CONSTANTS

The rovibrational constants used in this paper were obtained from a frequency analysis of the vibrational system $\nu_2/\nu_5/2\nu_3$. Therefore, a triad model enabled us to account accurately in a diagonalization all the interactions between the upper states of the three vibrational transitions. For $CH_3{}^{35}Cl$ and $CH_3{}^{37}Cl$ 4808 and 1706 individual rovibrational transitions, respectively, were used to determine the individual rovibrational constants. An additional 457 transitions were assigned for $CH_3{}^{35}Cl$ but not included in the determination of the constants since these lines were affected by blending. Assigned transitions involve $J' \leq 56$ for $CH_3{}^{35}Cl$ and $J' \leq 45$ for $CH_3{}^{37}Cl$. The analysis which includes Coriolis resonance between ν_2 and ν_5 as well as Fermi resonance between ν_5 and $2\nu_3$ is a restricted case of the formulation developed by Tarrago (9) for

analysis of up to five interacting bands. Relevant matrix elements are given by Tarrago *et al.* (10). The $2\nu_3$ band is very weak in our spectra and its' transitions have been assigned only in the region of a strong local perturbation with ν_5 around J' = 29. To facilitate the analysis, data on the ν_3 and $2\nu_3$-ν_3 bands obtained by Betrencourt *et al.* (11) were incorporated into our fits. Some 90 transitions with $41 \geq J' \geq 6$ were used. Since the $^RQ(J,0)$ branch of the ν_5 band is not clearly resolved on our spectra for $J'' \leq 36$, frequencies recorded with a diode laser by Henfrey and Thrush (12) were used despite the fact that a systematic offset of 0.001 cm^{-1} between ours and their frequency calibrations is suspected; this could not be confirmed because no resolved transitions from the two data sets could be directly compared. Our assignment of J values in $^RQ(J,0)$ confirms that previously given in Ref. (12) but it is different from that reported in Ref. (13) by two units in J. So the line assigned $^RQ(33,0)$ in Ref. (13) is assigned $^RQ(31,0)$ (and so on) here and in Ref. (12). The reason for the possible erroneous assignment in Ref. (13) could be due to the fact that the assignment was based on an analysis limited to J' = 30, whereas in the present work it is based on an analysis of ν_2 and ν_5 completed up to J' = 54. Because of the somewhat weak fit (especially at high J) we have obtained for the ν_5 band (standard deviation = 0.0013 cm-1) we think that the present assignment of $^RQ(J,0)$ up to J' = 57 can be questionable. This is probably due to the lack of a satisfactory set of data for $3\nu_3$ at high J and observe a weakness of the fit especially at high J and also the slight offset of line calibration in Ref. (12).

The ground state rotational constants resulting from the analysis are presented in Tables 3 and 4 for $CH_3{}^{35}Cl$ and $CH_3{}^{37}Cl$ respectively. The large correlation between A_0 and $D_0{}^K$ noted in Table 3 arises because only

sixteen ground state combination differences resulting from perturbation allowed transitions with $\Delta(k\text{-}l_5) = \pm 3$ could be retained in the fit. No perturbation-allowed transitions due to coupling between ν_2 and ν_5 or $2\nu_3$ and ν_5 were observed for $CH_3{}^{37}Cl$. Therefore, the $D_0{}^K$ value was constrained to the value calculated by Duncan (14). The rotational constants obtained for $CH_3{}^{35}Cl$ are in good agreement with the previous work of Di Lauro and Alamichel (15) as well as Jensen *et al.* (16); nevertheless, a slight disagreement can be observed for $D_0{}^K$, which is fixed in Ref. (15) to the value determined by Duncan (14) and determined in Ref. (16) from a simultaneous fit of both infrared and Raman spectra of the ν_4 band. For $CH_3{}^{37}Cl$ our results are also in good agreement with Ref. (15); the comparison in this case with Ref. (16) has no real meaning since in this reference only a tentative determination of A_0 was done due to a lack of line assignments. Note that A_0 of $CH_3{}^{35}Cl$ was also determined by Henfrey and Thrush (12) to equal 5.20569(9) cm^{-1}; in doing so they took other needed ground state rotational constants from previous work. Finally, we note that very accurate values of B_0, $D_0{}^J$, and $D_0{}^{JK}$ as well as sextic constants for $CH_3{}^{35}Cl$ and $CH_3{}^{37}Cl$ have been reported by Wlodarczak *et al.* (17). The latter paper contains references to previous microwave and sub-millimeter work.

Tables 5 and 6 give the excited state rotational constants and unperturbed vibrational band centers for $CH_3{}^{35}Cl$ and $CH_3{}^{37}Cl$ respectively. The parameters C and W found in these tables include interactions which involve respectively, two and three vibrational quanta. The superscripts on the C and W parameters indicate the vibrational quanta and the subscripts indicate $|\Delta K|$, $|\Delta l_5|$, and the order of the Hamiltonian involved. These constants were determined by holding fixed the respective ground-state

constants to the values given in Tables 3 and 4. For $2\nu_3$ of $CH_3{}^{37}Cl$, where only 5 line assignments are available, the parameters A, B, D were fixed to the ground state values. The related parameters of $2\nu_3$ for $CH_3{}^{35}Cl$ were not deemed appropriate because of the inversion of $2\nu_3$ and ν_5 positions in the two isotopic species. In the present work 28 excited state rovibrational constants were determined for the ν_2-ν_5-$2\nu_3$ complex of $CH_3{}^{35}Cl$; they include 21 diagonal and 7 off-diagonal contributions. Considering the different notations and phase conventions used for energy matrix elements, the results are in pretty good agreement with the results obtained by Morillon-Chapey (13) for $CH_3{}^{35}Cl$ and by Henfrey and Thrush (12) for $CH_3{}^{35}Cl$ and $CH_3{}^{37}Cl$. As expected the largest disagreements are between the highest order constants. This is in part probably due to the different models used for the fits. Also the vibrational band centers for ν_2 and $2\nu_3$ differ by more than ours and Henfrey and Thrush's uncertainties due to a different treatment of the Fermi resonance between ν_2 and $2\nu_3$. The difference between the sums of the ν_2 and $2\nu_3$ band center frequencies obtained here and by Henfrey and Thrush (12), however, is just 0.0322 cm^{-1}.

ν_2 AND ν_5 BAND INTENSITIES

On the basis of the wave functions obtained in fitting the observed frequencies and intensity measurements done on 24 $^{R}R(J,0)$ transitions in the ν_5 band (see Table 2) the ν_5 and ν_2 band intensities for $CH_3{}^{35}Cl$ are determined to be respectively 45.8(1.4) and 32.4(0.9) $cm^{-2}atm^{-1}$ at T = 296 K. To obtain these results we have summed line intensities up to J = 57 and K = 15 (2852 lines for ν_5 and 1440 lines for ν_2). Also, we have

assumed that the dipole moment derivative for the $2\nu_3$ band is equal to zero; $2\nu_3$ lines which appear in our listing derive their intensity from mixing with ν_5 transitions and the 440 lines computed have an integrated intensity of 0.22 $cm^{-2}atm^{-1}$. The comparable results for respectively the ν_5 and ν_2 bands of $CH_3{}^{37}Cl$ are 46.1(1.4) and 32.7(1.0) $cm^{-2}atm^{-1}$ (2553 lines for ν_5 and 1297 lines for ν_2).

To obtain the above intensity results we first assumed the dipole parameters obtained by Cappellani *et al.* (18). Then, we computed the individual line intensities and an appropriate scale factor was obtained as the average of the ratios of the measured intensities given in Table 2. and the calculated intensities. The band intensity was then calculated as the summation of the appropriate calculated line intensities multiplied by the factor 1.1307.

Our band ν_2 band intensity at T = 296 K for $CH_3{}^{35}Cl$ can be compared with that obtained via diode laser spectroscopy, Blanquet *et al.* (19) (33.46±0.13 $cm^{-2}atm^{-1}$) and Cappellani *et al.* (18) (29.9±0.9 $cm^{-2}atm^{-1}$) or via low-resolution measurements on natural samples, Kondo *et al.* (20) (34.6±2.8$cm^{-2}atm^{-1}$) and Elkins *et al.* (1) (37.0±1.5$cm^{-2}atm^{-1}$). Some of the previous band intensities obtained for the ν_5 band include Cappellani *et al.* (18) (39.7±0.4 $cm^{-2}atm^{-1}$) and Elkins *et al.* (1) (43.1±1.8 $cm^{-2}atm^{-1}$). Older measurements for both bands are referenced in Cappellani *et al.* (18).

SELF-BROADENING COEFFICIENTS

We measured self-broadening coefficients for 310 lines of $CH_3{}^{35}Cl$ and 123 lines of $CH_3{}^{37}Cl$. For $CH_3{}^{35}Cl$, 41 lines were ν_2 transitions and 269 ν_5 transitions. The broadening coefficients were measured in order to

determine the diagonal elements of the relaxation matrix which is required for the collisional-line-mixing calculations discussed below. All of the measured $CH_3{}^{35}Cl$ broadening coefficients plotted versus the lower state rotational quantum number, J, are shown in Fig. 1. The broadening coefficients were determined in the J and K ranges, $0 \geq J \geq 42$ and $0 \geq K \geq 8$, respectively. Broadening results for $CH_3{}^{37}Cl$ are not shown but fall in the same range as shown in Fig. 1 with a little more scatter. In Fig. 1 the broadening coefficients are observed to decrease rapidly from J = 0 to J = 3 then increase to peak broadly between J = 14-17 and then to decrease steadily with increasing J. This qualitative behavior can be contrasted with N_2 (21) and O_2 (22) broadening in the ν_3 band of $CH_3{}^{35}Cl$ where the broadening simply decreases as J increases. The broad maximum is characteristic of broadening enhanced by resonant-self collisions between like molecules with large permanent electric dipole moments; such behavior has been clearly associated in HCl (23) with the maximum of the quantity $(2J+1)\exp(-E''/kT)$, (where E" is the lower state energy), which for $CH_3{}^{35}Cl$ occurs at J = 15. Self-broadening measurements and associated Anderson-type calculations for the ν_3 band of $CH_3{}^{35}Cl$ (2-3, 24) also show the same broad maximum but were not done at the low J values, J = 0 - 3. The full range of broadening behavior we have observed for $CH_3{}^{35}Cl$ has also been observed and calculated (25,26) for CH_3F. The Boltzmann maximum for CH_3F, however, occurs at about J = 11 but the observed J dependence of the broadening is about the same as for CH_3Cl. The calculations of the broadening done for CH_3Cl and CH_3F did not include the J" = 0-3 quantum numbers. Calculations of self-broadening coefficients done by Blanquet *et al.* (3) for $^{Q}R(J,K)$ transitions indicate that for a given J that $\gamma(J,K)$ should decrease uniformly with K; their small number of

measurements confirmed this predicted trend. Except for $^{R}R(J,0)$ and $^{R}R(J,1)$ transitions we have not clearly observed such a K trend among the other transitions we have measured.

$^{R}Q(J,0)$ COLLISIONAL LINE MIXING

The line shape and frequency parameters which we obtained, as described above, were used to calculate spectra over the region of the $\nu_2/\nu_5/2\nu_3$ triad. Parameters used for the $^{R}Q(J,0)$ branch are specifically given in Table 8. Overlapping Voigt line profile were used to calculate the absorption coefficients used for these preliminary calculations although, since the self-broadening coefficients are so large, a Lorentzian profile is adequate to model spectra recorded at pressures as low as 13.7 torr. The agreement between the calculated and observed transmission spectra was excellent for most of the ν_5 band as well as the ^{Q}P and ^{Q}Q branches of the ν_2 band which we checked. There is perhaps a small amount of line mixing evident in the $^{P}Q(J,1)$ and $^{R}Q(J,K=2,3)$ (K=1 not observed) branches of the ν_5 band. Figure 2 shows a very typical comparison between observed and calculated spectra, here for the $^{R}Q(J,8)$ branch. On the other hand the very dense $^{R}Q(J,0)$ branch of the ν_5 band can not be well calculated with overlapping Voigt profiles unless the pressure is low enough for collisional effects to be unimportant.

Figure 3 compares the observed and calculated $^{R}Q(J,0)$ branch transmission recorded at a gas pressure of 0.719 torr; here the agreement is very good. However, as can be seen in Figs. 4 and 5, recorded at 13.74 and 23 torr respectively, there is an obvious problem with the calculations matching the observations very well. Since the $^{R}Q(J,0)$ branches in the ν_5

band of $CH_3{}^{35}Cl$ and $CH_3{}^{37}Cl$ are so dense we assumed that a calculation of the absorption coefficient which includes collisional line mixing would afford a better model for this spectral feature. An underlying assumption of the calculations, the impact approximation, is well satisfied since the width of this Q-branch feature is on the order of 0.6 cm^{-1} while $1/(2\pi\tau_c)$ = 9 cm^{-1}, where τ_c is the duration of a collision. Other approximations are pointed out below.

Transmission spectra were calculated using the Beer-Lambert law,

$$T(\sigma) = \exp[-\alpha(\sigma)L], \tag{1}$$

where σ is the wave number, L the optical path length of the absorption cell, and $\alpha(\sigma)$ the absorption coefficient. Since the $^{R}Q(J,0)$ branch could not be well reproduced if overlapping Voigt profiles were used to calculate the absorption coefficient we invoked collisional line mixing .

The first order formulation of collisional line mixing derived by Rosenkranz (27) was used to calculate the absorption coefficient. Here the absorption coefficient is the sum of Lorentzian and mixing terms,

$$\alpha(\sigma) = \alpha_{Lor}(\sigma) + \alpha_{mix}(\sigma), \tag{2}$$

where

$$\alpha_{Lor}(\sigma) = \sum_i \frac{S_i}{\pi}\frac{\sigma}{\sigma_i}\frac{\gamma_i}{(\sigma-\sigma_i)^2+\gamma_i^2} \tag{3}$$

and

$$\alpha_{mix}(\sigma) = \sum_i \frac{S_i}{\pi}\frac{\sigma}{\sigma_i}\frac{(\sigma-\sigma_i)Y_i}{(\sigma-\sigma_i)^2+\gamma^2}\,. \tag{4}$$

The individual line intensities, S_i, and line positions, σ_i, were taken from the calculations and measurements described above. Parameters used for the $^{R}Q(J,0)$ branch are given in Table 8. The broadening coefficients, γ_i,

were least-squares fitted form the self-broadening coefficients shown in Fig. (1) assuming a polynomial dependence upon initial initial rotational quantum numbers J_i: $\gamma_i = \sum_{n=0}^{5} c_n J_i^n$. We assume here that the pressure broadening coefficients measured for isolated lines outside the $^RQ(J,0)$ branch will give a good representation of the broadening coefficients within the branch. The line mixing parameters, Yi, representing the coupling between line i and all other lines of the branch were computed according to

$$Y_i = 2 \sum_{j \neq i} \frac{\mu_j}{\mu_i} \frac{W_{ji}}{\sigma_i - \sigma_j} \tag{5}$$

where μ_i and μ_j are the dipole moments of lines i and j, respectively. The W_{ji} parameters were computed from the inelastic rates via

$$W_{ji} = -pK(i \rightarrow j) \tag{6}$$

with p the gas pressure, J_i and J_j initial rotational quantum numbers of lines i and j, respectively. The upward inelastic rates, K(jj'), were assumed to be well described via a MEG scaling law (28,29),

$$K(j \rightarrow j') = a_1 \left[\frac{1 + a_4 \left(E_j / a_2 kT \right)}{1 + a_4 \left(E_j / kT \right)} \right]^2 \exp\left(- \frac{a_3 \left| \Delta E_{jj'} \right|}{kT} \right), \tag{7}$$

while the downward rates were calculated from the expression for detailed balance:

$$K(j' \rightarrow j) = \frac{2j+1}{2j'+1} K(j \rightarrow j') \exp\left(\frac{\Delta E_{jj'}}{kT}\right), \quad (8)$$

where $\Delta E_{jj'}$ is the difference between the rotational energy levels E_j and $E_{j'}$. The inelastic rate coefficients, a_i, were calculated by least-squares fitting the γ_i to the sum rule expression,

$$\gamma(j) = \frac{1}{2}\left[\sum_{\substack{j_i' \neq j \\ (A^+)}} K\left(j \rightarrow j_i'\right) + \beta^- \sum_{\substack{j_f' \neq j \\ (A^-)}} K\left(j \rightarrow j_f'\right) + \beta^+ \sum_{\substack{j_f' \neq j \\ (A^+)}} K\left(j \rightarrow j_f'\right)\right], \quad (9)$$

where β^+ and β^- are numerical parameters ($\beta^+ + \beta^- = 1$). The fitted parameters, a_i, are presented in Table 9. Eq. (9) assumes that elastic reorientational collisional processes are not important processes for determining the line shape. We estimate that about 14% and 4% respectively of the collisions CH_3Cl experiences in the J, K = 1, 1 and 2,1 states are reorientational. The corresponding cross sections are 100 $Å^2$ and 32 $Å^2$ for $\Delta m = \pm 1$ reorientational collisions out of the J, K = 1, 1 and 2, 1 states respectively. These cross sections can be compared with the cross section of 759 $Å^2$ which corresponds to a pressure broadening coefficient of 0.5 cm^{-1}/atm. These estimates are based on measurements made by Shoemaker *et al.* (30) on CH_3F which has a large permanent electric dipole moment nearly equal to that of CH_3Cl. We have also assumed, as Anderson (31) has shown, that the matrix element squared for reorientational collisionals between orientated dipoles is given by $|\langle J,K,M|H_{dipole}|J,K,M\pm1\rangle|^2 \propto \{K^2(J\pm M+1)(J\mp M)/J(J+1)^2\}$.

The derivation of Eqs. (2-5) assumes that the W_{ij} are small compared to the $(\sigma_i - \sigma_j)$ quantities . This is not the case for the largest of the values of

these quantities determined at the highest pressure (23 torr) for transitions at the Q-branch head where $W_{01}/(\sigma_0-\sigma_1) \approx 1.4$. The validity of the Rosenkranz first order development (27) has been discussed in Ref. 34 for the case of CO_2.

Equation 9 was evaluated with unrestricted collisional selection rules on ΔJ with $J \leq 57$ and $\Delta K = 0$ ($J \leq 45$ for $CH_3{}^{37}Cl$) . The first term in Eq. (9) refers to the ground vibrational state which has only A^+ levels. The J levels of the upper state of ν_5 $^RQ(J,0)$ transitions ($K' = 1$), however, are each split into A^+ and A^- levels. The optical selection rule for these $^RQ(J,0)$ transitions is $A^+ \leftrightarrow A^-$. The absorption coefficient of the $^RQ(J,0)$ branch was calculated under two assumptions on the collsional relaxation allowed in the excited state of ν_5. With $\beta^- = 1$ and $\beta^+ = 0$ only $A^- \leftrightarrow A^-$ collisional relaxation is allowed in the excited states of the $^RQ(J,0)$ transitions, but with $\beta^-= 0.5$ and $\beta^+= 0.5$ both $A^- \leftrightarrow A^-$ and $A^- \leftrightarrow A^+$ collisions are allowed to occur with equal probability. Examination of both Figs. 4 and 5 panels d and e shows that a better fit to the data is obtained with the relaxed collisional selection rules. The overall rotational energy transfer (RET) collisional selection rules we have assumed, $\Delta K = 0$, $|\Delta J| \geq 1$, seem reasonable since time-resolved double-resonance (microwave-infrared) measurements of rotational energy transfer in CH_3Cl (32) show that the comparable cross sections for $\Delta K=3n$ (n=1, 2...) RET are on the order one to two orders of magnitude smaller. On the other hand more channels would be accessible thru these processes. Individual Y values determined for these two cases are given in Table 10. The residual discrepancies in the Figs. 4 and 5 of about 4 percent are comparable to what for CO_2 (33) and N_2O (34) has been attributed to use of the Rosenkranz approximation (27). To make this comparison we note that these molecules have rotational B

values comparable to CH_3Cl but also that CO_2 has only J even allowed in it's ground state.

CONCLUSIONS

Spectra calculated using overlapping Voigt profiles and line-intensity, -position and -broadening parameters obtained in this work for the ν_5 band of $CH_3{}^{35}Cl$ and $CH_3{}^{37}Cl$ give a quantitative representation of the band except notably for the $^RQ(J,0)$ branch which is formed by the near superposition of a number of individual lines. The $^RQ(J,0)$ branch, however, can be adequately modeled by a simple line mixing model. If optical selection rules are applied to the line mixing model (transitions between like parity states forbidden) then too much mixing results. However, the $^RQ(J,0)$ branch can be well modeled if equal probability is given to parity-changing and parity-conserving $\Delta K = 0$, $|\Delta J| \geq 1$ collisional transitions. It is possible, however, that our inclusion of parity-changing collisions makes up for our neglect of a large number of $\Delta K \neq 0$ ($\Delta(\pm K) = 3n$) collisions. The self-broadening coefficients peak at the maximum of the ground state Boltzmann population distribution, J" = 14-15; this is characteristic of resonant dipole collisions as the major contributor to the broadening process.

An extensive list of assigned lines and frequencies for the 1261 - 1645 cm^{-1} region of methyl chloride has been tabulated for presentation in the HITRAN and GEISA data bases. Accurate ground and excited state constants have been determined for the (ν_2, ν_5 ,$2\nu_3$)-vibrational-band triad.

ACKNOWLEDGEMENTS

To Claude Plymate at the National Solar Observatory for assistance in obtaining the spectra. C. Chackerian acknowledges the hospitality afforded by the Universitiés Pierre et Marie Curie Paris (6) and Paris-Sud (11). Part of the research reported in this paper was performed at the Jet Propulsion Laboratory, California Institute of Technology, under contract with the National Aeronautics and Space Administration.

REFERENCES

1. J. W. Elkins, R. H. Kagan, and R. L. Sams,
J. Mol. Spectrosc. **105**, 480-490 (1984).

2. J. -P. Bouanich, G. Blanquet, and J. Walrand,
J. Quant. Spectrosc. Radiat. Trans. **51**, 573-578 (1994).

3. G. Blanquet, J. Walrand, J.-C. Populaire, and J.-P. Bouanich,
J. Quant. Spectrosc. Radiat. Trans. **53**, 211-219 (1995).

4. J. -M. Hartman, J. -P. Bouanich, C. Boulet, Gh. Blanquet, J Walrand, and N. *Lacome, J. Quant. Spectrosc. Radiat. Trans.* **54**, 723-735 (1995).

5. Fr. Frichot, N. Lacome and J.-M. Hartmann,
J. Mol. Spectrosc. **178**, 52-58 (1996).

6. M. N. Spencer, C. Chackerian, Jr., L. P. Giver and L. R. Brown,
J. Mol. Spectrosc. **165**, 506-524(1994).

7. L. R. Brown and R. A. Toth, *J. Opt. Soc. Am.* **B2**, 842-856 (1985).

8. L. R. Brown, J. S. Margolis, R. H. Norton and B. D. Stedry,
Appl. Spectr. **37**, 287-292 (1983).

9. G. Tarrago, *J. Mol. Spectrosc.* **139**, 439-445 (1990).

10. G. Tarrago, N. Lacome, A. Levy, G. Guelachvili, B. Bezard and P. Drossart,
J. Mol. Spectrosc. **154**, 30-42 (1992).

11. M. Betrencourt, M. Morillon-Chapey, G. Blanquet and J. Walrand, *J. Mol. Spectrosc.* **128**, 433-443 (1988).

12. N. F. Henfrey, and B. A. Thrush *J. Mol. Structure*, **146**, 71-83 (1986).

13. M. Morillon-Chapey, G. Guelachvili and P. Jensen, *Can. J. Phys.* **62**, 247-253 (1984).

14. J. L. Duncan, *J. Mol. Spectrosc.* **60**, 225-238 (1976).

15. C. Di Lauro and C. Alamichel, *J. Mol. Spectrosc.* **81**, 390-412 (1980).

16. P. Jensen, S. Brodersen and G. Guelachvili, *J. Mol. Spectrosc.* **88**, 378-393 (1981).

17. G. Wlodarczak, D. Boucher, R. Bocquet and J. Demaison, *J. Mol. Spectrosc.* **116**, 251-255 (1986).

18. F. Cappellani, G. Restelli and G. Tarrago, *J. Mol. Spectrosc.* **146**, 326-333 (1991).

19. G. Blanquet, B. Lance, J. Walrand and J.-P. Bouanich, *J. Mol. Spectrosc.* **170**, 466-477 (1995).

20. S. Kondo, Y. Koga, T. Nakanaga, and S. Saeki, *Bull. Chem. Soc. Japan* **56**, 416-421 (1983).

21. G. Blanquet, J. Warland, and J.-P. Bouanich, *J. Mol. Spectrosc.***160**, 253-257 (1993).

22. G. Blanquet, J. Warland, and J.-P. Bouanich, *J. Mol. Spectrosc.***159**, 137-143 (1993).

23. C. Chackerian, Jr., D. Goorvitch, and L. P. Giver, *J. Mol. Spectrosc.* **113**, 373-387 (1985).

24. G. Blanquet, P. Coupe, J. Walrand, and J. P.- Bouanich, *J. Quant. Spectrosc. Radiat. Trans.* **51**, 671-678 (1994).

25. D. Guerin, M. Nischan, D. Clark, V. Dunjko, and A. Mantz, *J. Mol. Spectrosc.* **166**, 130-136 (1994).

26. B. Lance, M. Lepere, G. Blanquet, J. Warland and J.-P. Bouanich, *J. Mol. Spectrosc.* **180**, 100-109 (1996).

27. P. W. Rosenkranz, *IEEE Trans. Antennas Propag.* **AP-23**, 498-506 (1975).

28. L. A. Rahn and R. E. Palmer, *J. Opt. Soc. Am.* **B3**, 1164-1169 (1986).

29. M. L. Koszykowski, M. L. Rahn, R. E. Palmer, and M. E. J. Coltrin, *J. Phys. Chem.* **91**, 41-46 (1987).

30. R. L. Shoemaker, S. Stenholm and R. Brewer, *Phys. Rev.* **A10**, 2037-2050 (1974).

31. P. W. Anderson, *Phys. Rev.* **76**, 647-661 (1947).

32. T. W. Pape, F. C. De Lucia, and D. D. Skatrud, *J. Chem. Phys.* **100**, 5666-5683 (1994).

33. B. Gentry and L. L. Strow and , *J. Chem. Phys.* **86**, 5722-5730 (1987).

34. L. L. Strow and A. S. Pine, *J. Chem. Phys.* **89**, 1427-1434 (1988).

TABLE TITLES

1. Experimental Conditions.

2. $CH_3{}^{35}Cl$ ν_5 $^RR(J,0)$ Measured Positions Strengths and Widths.

3. Ground State Rotational Constants (in cm^{-1}) for $CH_3{}^{35}Cl$.

4. Ground State Rotational Constants (in cm^{-1}) for $CH_3{}^{37}Cl$.

5. Spectroscopic Constants (in cm^{-1}) for the ν_2, ν_5 ,$2\nu_3$ Triad of $CH_3{}^{35}Cl$.

6. Spectroscopic Constants (in cm^{-1}) for the ν_2, ν_5 ,$2\nu_3$ Triad of $CH_3{}^{37}Cl$.

7. Band intensities of $CH_3{}^{35}Cl$.

8. Frequency and Intensity Parameters for $^RQ(J,0)$ of $CH_3{}^{35}Cl$ and $CH_3{}^{35}Cl$ of the ν_5 Vibrational Band.

9. MEG Scaling Law Parameters.

10. Broadening and Mixing Coefficients.

TABLES

TABLE 1. Experimental Conditions.

Path(cm)	Pressure(Torr)	Temperature(K)	Band Pass (cm^{-1})
25.0	0.222	294.7	1000-2700 cm^{-1}
25.0	0.719	295.3	" "
150.0	0.206	295.7	" "
150.0	0.6610	295.9	" "
25.0	7.988	296.2	" "
25.0	13.750	296.3	" "
2.63	23.1	296.0	550 - 2700 cm^{-1}
2.63	8.6	296.0	" "

TABLE 2. $CH_3{}^{35}Cl$ ν_5 $^RR(J,0)$ Measured[a] Positions Strengths[b] and Widths.

J"	σ(High P) rms (cm^{-1})	Diff(H-L)[c] (cm^{-1})	S(low P) (cm^{-2}/atm)	S(high P) (cm^{-2}/atm)	%Diff. (H-L)	Self γ (cm^{-1}/atm)	%Err.
0	1460.40581 (44)	0.00035	0.0123	0.0111	-10.0	0.574	11.1
1	1461.30808 (07)	0.00030	0.0188	0.0188	-0.1	0.490	0.1
2	1462.21849 (10)	0.00027	0.0271	0.0274	1.2	0.482	10.0
3	1463.13584 (28)	0.00015	0.0328	0.0312	-4.9	0.422	2.6
4	1464.06032 (04)	-0.00004	0.0390	0.0403	3.4	0.452	5.3
6	1465.92989 (43)			0.0523		0.442	3.8
7	1466.87349 (39)			0.0577		0.488	4.9
8	1467.82335 (14)	0.00016	0.0607	0.0627	3.3	0.487	3.4
9	1468.77847 (17)	0.00012	0.0683	0.0686	0.4	0.501	2.7
10	1469.73940 (23)	0.00008	0.0702	0.0722	2.9	0.528	4.3
11	1470.70546 (03)	0.00013	0.0724	0.0734	1.4	0.533	0.7
16	1475.61095 (04)	0.00002	0.0799	0.0809	1.2	0.572	2.8
17	1476.60675 (06)	0.00016	0.0814	0.0825	1.3	0.582	0.5
18	1477.60708 (19)	0.00009	0.0769	0.0778	1.1	0.560	2.8
19	1478.61198 (06)	-0.00003	0.0749	0.0769	2.7	0.567	3.0
21	1480.63591 (06)	0.00004	0.0707	0.0689	-2.6	0.512	3.4
22	1481.65459 (02)	-0.00004	0.0682	0.0679	-0.6	0.512	2.0
23	1482.67719 (08)	-0.00023	0.0749	0.0761	1.6	0.494	5.6
26	1485.77366 (08)	0.00009	0.0563	0.0549	-2.4	0.427	4.9
27	1486.81412 (21)	-0.00003	0.0515	0.0529	2.9	0.438	2.7
28	1487.85844 (28)	-0.00020	0.0458	0.0467	2.3	0.401	2.5
31	1491.01661 (04)	-0.00005	0.0353	0.0356	0.8	0.357	9.8
32	1492.07719 (10)	-0.00005	0.0330	0.0306	-7.6	0.310	2.2
37	1497.43482 (08)	-0.00060	0.0181	0.0187	3.2	0.248	6.9

[a]The absolute accuracies are ± 0.0002 cm^{-1} for positions and ± 3% for widths and strengths.

[b]The strengths observed in natural isotopic abundance have been scaled to their values corresponding to a 100% ^{35}Cl sample by applying the factor 1.335x.

[c]The conditions of low (L) and high (H) pressure runs are listed in Table 1.

TABLE 3. Ground State Rotational Constants[a] (in cm^{-1}) for $CH_3{}^{35}Cl$.

Parameter	This work	Ref. (15)	Ref. (16)
B_0	0.44340326(27)	0.4434041(6)	0.4434026(12)
A_0	5.20752(11)[b]	5.20531(11)	5.205304(97)
$D_0^J x10^7$	6.04588(92)	6.045(4)	6.0302(81)
$D_0^{JK} x10^6$	6.6004(37)	6.641(17)	6.555(53)
$D_0^K x10^4$	1.168(17)[b]	0.8342[c]	0.885(13)
Combination differences	2681 ($J \leq 54$)	1231	538
r.m.s. (in cm^{-1})	0.0004	0.0006	0.0007

[a]Errors in parenthesis represent one standard deviation.
[b]These two parameters are highly correlated in the fit, cc = 0.9992.
[c]Constrained to the value given in Ref.(14)

TABLE 5. Spectroscopic Constants[a] (in cm^{-1}) for the ν_2, ν_5 ,$2\nu_3$ Triad of $CH_3{}^{35}Cl$.

Parameter	$2\nu_3$	ν_2	ν_5
ν	1456.76217(16)	1354.881443(86)	1452.181030(60)
B_v	0.43572825(50)	0.44214018(26)	0.44356988(16)
A_v	5.1905892(54)	5.2305207(29)	5.1615532(18)
$(A\zeta)_v$			-1.3057725(53)
$D_v{}^J x10^7$	6.0740(28)	6.07688(79)	6.10962(53)
$D_v{}^{JK} x10^6$	6.6009(70)	6.5620(19)	6.4742(13)
$D_v{}^K x10^4$	1.15617(26)	1.20076(18)	1.14690(10)
$\eta_J x10^5$			-1.44166(95)
$\eta_K x10^6$			-5.622(90)
Transitions	391	1469 ($J' \leq 56$)	2948 ($J' \leq 59$)
Std. dev. of fit	0.0010 cm^{-1}	0.0008 cm^{-1}	0.0013 cm^{-1}
ν_2/ν_5 Coriolis	$\left(C_{111}^{25}\right)^* = 0.271016(92)$, $C_{112}^{25} = -1.09591(53)10^{-3}$, $C_{113J}^{25} = -6.891(22)10^{-7}$, $C_{212}^{25} = 2.2580(19)10^{-4}$		
$\nu_5/2\nu_3$ Fermi	$W_{112}^{533} = 3.79438(94)10^{-2}$, $W_{113}^{533} = 6.174(43)10^{-4}$, $W_{213}^{533} = -5.019(49)10^{-5}$.		

[a]Notation is according to Refs. (9-10). For example, all the W^{533} coefficients are related to the Fermi interaction between ν_5 and $2\nu_3$; the leading term, W_{112}^{533}, arises from the second order Hamiltonian term, $r_5 r_3^2 P$, (indicated by the two in third subscript). The first two subscripts, 11, indicate that $\Delta K = \pm 1$ and $\Delta l = \pm 1$ transitions respectively are involved. The errors are quoted for one standard deviation. The results of the fit are unchanged if the signs of all the off-diagonal elements are reversed. The overall standard deviation of the fit is equal to 0.0011 cm^{-1} for the 4808 transitions fitted. Ground state parameters used for this fit are taken from Table 3.

$$\left(C_{111}^{25}\right)^* = C_{111}^{25} + C_{113n}^{25} + C_{113t0},$$

$$C_{111}^{25} = \left\{\left(B_e \zeta_{25}^{(x)}/2\right)\right\}\left\{\left(\omega_2 + \omega_5\right)/\left(\omega_2\omega_5\right)^{1/2}\right\}.$$

TABLE 4. Ground State Rotational Constants[a] (in cm^{-1}) for $CH_3{}^{37}Cl$.

Parameter	This work	Ref. (15)	Ref. (16)
B_0	0.43657491(89)	0.436575(2)	0.436575[c]
A_0	5.203035(24)	5.20317(19)	5.2182(10)
$D_0^J x10^7$	5.8666(45)	5.91(2)	5.91[c]
$D_0^{JK} x10^6$	6.470(22)	6.46(6)	6.46[c]
$D_0^K x10^4$	8.342(17)b	8.342[b]	0.885[d]
Combination differences	631 (J≤45)	558	
r.m.s. (in cm^{-1})	0.0006	0.0009	

[a]Errors in parenthesis represent one standard deviation.
[b]Constrained to the value given in Ref. (14).
[c]Constrained to the value of Ref. (15).
[d]Constrained to the value determined for $CH_3{}^{35}Cl$ in Ref. (16).

TABLE 6. Spectroscopic Constants[a] (in cm^{-1}) for the ν_2, ν_5 ,$2\nu_3$ Triad of $CH_3{}^{37}Cl$.

Parameter	$2\nu_3$	ν_2	ν_5
ν	1445.35168(46)	1354.69111(10)	1452.152546(71)
B_v	0.43657491[b]	0.4353149(11)	0.43672777(55)
A_v	5.203035[b]	5.2259912(43)	5.1573127(35)
$(A\zeta)_v$			-1.3101089(88)
$D_v{}^J x10^7$	5.8666[b]	5.9178(24)	5.9190(14)
$D_v{}^{JK} x10^6$	6.470[b]	6.4320(33)	6.3852(32)
$D_v{}^K x10^5$	8.342[b]	8.6857(33)	8.1454(29)
$\eta_J x10^5$			-1.3579(21)
$\eta_K x10^4$			-1.4694(23)
ν_2/ν_5 Coriolis	$\left(C_{111}^{25}\right)^* = 0.266294(48)$, $C_{112}^{25} = -1.0512(31)10^{-3}$, $C_{111J}^{25} = -7.992(77)10^{-7}$, $C_{212}^{25} = 2.2070(46)10^{-4}$.		
$\nu_5/2\nu_3$ Fermi	$W_{112}^{533} = 4.0704(14)10^{-4}$.		
Transitions	5($31 \le J' \le 36$)	554($J' \le 45$)	1147($J' \le 45$)
Std. dev. of fit	0.0025 cm^{-1}	0.0007 cm^{-1}	0.0011 cm^{-1}

[a]See Footnote a of Table 5 for explanation of notation.
[b]Fixed to ground state values.
The overall standard deviation of the fit is equal to 0.0010 cm^{-1} for the 1706 transitions involved. ($J' \le 45$).
Ground state parameters used for this fit are taken from Table 4.

TABLE 7. Band Intensities[a] of $CH_3{}^{35}Cl$.

Reference	ν_2 band	ν_5 band
Cappellani *et al.* (18)	29.9(0.9)	39.7(1.1)
Blanquet *et al.* (19)	33.46(0.13)	
Kondo *et al.* (20)	33.0(2.7)	
Elkins *et al.* (1)	37.0(1.5)	43.1(1.8)
Present	32.4(0.9)	45.8(1.4)

[a]At 296 K. Units of band intensity are (cm^{-1}/cm-atm).

TABLE 8. Frequency[a] and Intensity Parameters for $^{R}Q(J,0)$ of $CH_3{}^{35}Cl$ and $CH_3{}^{35}Cl$ of the ν_5 Vibrational Band.

	$CH_3{}^{35}Cl$				$CH_3{}^{37}Cl$		
J"	σ (cm^{-1})	(o-c)[b]	Intensity (cm^{-2}/atm)	GS energy (cm^{-1})	σ (cm^{-1})	Intensity (cm^{-2}/atm)	GS energy (cm^{-1})
1	c1459.51073		0.173E-01	0.88680	c1459.49338	0.173E-01	0.87315
2	c1459.51131		0.286E-01	2.66040	c1459.49392	0.286E-01	2.61943
3	c1459.51219		0.395E-01	5.32075	c1459.49472	0.395E-01	5.23881
4	c1459.51335		0.499E-01	8.86782	c1459.49578	0.499E-01	8.73126
5	c1459.51481		0.597E-01	13.30155	c1459.49710	0.598E-01	13.09672
6	c1459.51655		0.688E-01	18.62187	c1459.49870	0.688E-01	18.33511
7	c1459.51858		0.770E-01	24.82869	c1459.50055	0.771E-01	24.44636
8	c1459.52091		0.843E-01	31.92190	c1459.50267	0.845E-01	31.43035
9	c1459.52351		0.906E-01	39.90140	c1459.50505	0.909E-01	39.28699
10	c1459.52641		0.959E-01	48.76704	c1459.50769	0.963E-01	48.01614
11	1459.52920	-3.8	0.100E+00	58.51870	c1459.51059	0.101E+00	57.61767
12	1459.53270	-3.5	0.103E+00	69.15620	c1459.51376	0.104E+00	68.09141
13	c1459.53679		0.106E+00	80.67937	c1459.51718	0.106E+00	79.43720
14	1459.53990	-9.2	0.107E+00	93.08802	c1459.52086	0.108E+00	91.65486
15	1459.54440	-7.2	0.107E+00	106.38196	c1459.52479	0.108E+00	104.74419
16	1459.54880	-9.0	0.106E+00	120.56096	c1459.52898	0.107E+00	118.70497
17	1459.55400	-5.6	0.105E+00	135.62479	c1459.53342	0.106E+00	133.53699
18	1459.55900	-6.9	0.103E+00	151.57320	c1459.53812	0.104E+00	149.24000
19	1459.56320	-18.8	0.996E-01	168.40594	c1459.54306	0.101E+00	165.81375
20	1459.56940	-13.5	0.961E-01	186.12272	c1459.54824	0.974E-01	183.25798
21	1459.57520	-14.8	0.920E-01	204.72326	c1459.55368	0.935E-01	201.57239
22	1459.58180	-10.6	0.876E-01	224.20726	c1459.55935	0.891E-01	220.75670
23	1459.58830	-10.2	0.829E-01	244.57438	c1459.56527	0.844E-01	240.81059
24	1459.59450	-15.2	0.779E-01	265.82431	c1459.57142	0.795E-01	261.73375
25	1459.60080	-21.8	0.728E-01	287.95668	c1459.57780	0.744E-01	283.52583
26	1459.60790	-22.7	0.677E-01	310.97115	c1459.58442	0.693E-01	306.18648
27	1459.61510	-25.3	0.625E-01	334.86732	c1459.59127	0.641E-01	329.71534
28	1459.62370	-16.1	0.575E-01	359.64482	c1459.59834	0.590E-01	354.11202
29	1459.63130	-19.3	0.525E-01	385.30323	c1459.60564	0.540E-01	379.37613
30	1459.63940	-19.8	0.477E-01	411.84213	c1459.61315	0.492E-01	405.50727
31	1459.64750	-22.6	0.431E-01	439.26109	c1459.62089	0.446E-01	432.50500
32	1459.65640	-19.7	0.388E-01	467.55965	c1459.62883	0.402E-01	460.36890
33	1459.66450	-26.8	0.347E-01	496.73736	c1459.63698	0.360E-01	489.09851
34	1459.67410	-21.2	0.309E-01	526.79373	c1459.64533	0.321E-01	518.69338
35	1459.68340	-20.6	0.273E-01	557.72827	c1459.65388	0.285E-01	549.15301
36	1459.69230	-26.0	0.241E-01	589.54047	c1459.66263	0.252E-01	580.47692
37	1459.70250	-20.3	0.211E-01	622.22982	c1459.67157	0.221E-01	612.66460
38	1459.71245	-19.0	0.184E-01	655.79577	c1459.68070	0.193E-01	645.71552
39	1459.72261	-17.4	0.160E-01	690.23777	c1459.69000	0.168E-01	679.62917
40	1459.73335	-11.9	0.138E-01	725.55525	c1459.69948	0.146E-01	714.40498
41	1459.74325	-16.3	0.119E-01	761.74765	c1459.70913	0.125E-01	750.04239
42	1459.75402	-13.8	0.101E-01	798.81435	c1459.71896	0.108E-01	786.54082
43	1459.76468	-13.8	0.862E-02	836.75476	c1459.72893	0.918E-02	823.89969
44	1459.77591	-9.6	0.730E-02	875.56824	c1459.73907	0.780E-02	862.11839

45	1459.78683	-10.0	0.616E-02	915.25416	c1459.74935	0.659E-02	901.19629
46	1459.79797	-9.4	0.517E-02	955.81187			
47	1459.81020	0.8	0.432E-02	997.24068			
48	1459.82113	-3.0	0.359E-02	1039.53996			
49	1459.83258	-2.8	0.297E-02	1082.70896			
50	1459.84477	4.0	0.244E-02	1126.74699			
51	1459.85693	9.7	0.200E-02	1171.65333			
52	1459.86944	18.1	0.164E-02	1217.42723			
53	1459.88127	19.3	0.133E-02	1264.06794			
54	1459.89538	42.8	0.107E-02	1311.57469			
55	1459.90822	53.3	0.865E-03	1359.94669			
56	1459.91923	45.6	0.693E-03	1409.18316			
57	c1459.92644		0.553E-03	1459.28327			

[a]Observed value, or calculated one if letter c appears.
[b]Observed minus calculated values in units of 10^{-4} cm^{-1}.

TABLE 9. MEG Scaling Law Parameters[a].

MEG Law Parameter	$\beta^- = 1.0; \beta^+ = 0.0$	$\beta^- = \beta^+ = 0.5$
a_1	0.0390[b]	0.0262[b]
a_2	0.548[c]	0.547[c]
a_3	2.69[c]	2.70[c]
a_4	2.45[c]	2.31[c]

[a]These parameters appear in Eq. 5.
[b]Units are cm^{-1}/atm.
[c]Units are dimensionless.

TABLE 10. Broadening and Mixing Coefficients.

J"	γ_o	$Yo(A^{\pm} \leftrightarrow A^{\pm})$	$Yo(A^{\pm} \leftrightarrow A^{\pm}, A^{+} \leftrightarrow A^{-})$
1	0.4015	290.3991	194.7278
2	0.4041	92.5850	61.9914
3	0.4097	62.2638	41.6384
4	0.4177	46.5380	31.0829
5	0.4275	27.9626	18.6317
6	0.4386	18.7964	12.4953
7	0.4505	11.6947	7.7482
8	0.4627	13.9592	9.2732
9	0.4750	6.1276	4.0441
10	0.4869	2.1579	1.4007
11	0.4980	-1.4235	-0.9835
12	0.5081	-0.8225	-0.5711
13	0.5168	3.9781	2.6515
14	0.5241	-14.6480	-9.8020
15	0.5296	-5.3360	-3.5636
16	0.5332	-11.4734	-7.6667
17	0.5349	-3.9058	-2.5976
18	0.5344	-1.4352	-0.9372
19	0.5318	-23.7412	-15.8688
20	0.5271	-9.3100	-6.2032
21	0.5202	-13.5660	-9.0543
22	0.5113	-8.7679	-5.8410
23	0.5003	-7.6396	-5.0849
24	0.4875	-10.9171	-7.2791
25	0.4731	-14.9608	-9.9875
26	0.4571	-12.5538	-8.3743
27	0.4399	-15.3892	-10.2765
28	0.4217	-7.3570	-4.8950
29	0.4028	-11.3447	-7.5696
30	0.3836	-10.4344	-6.9596
31	0.3645	-12.1929	-8.1395
32	0.3458	-8.2735	-5.5123
33	0.3280	-13.7252	-9.1686
34	0.3117	-9.1191	-6.0814
35	0.2972	-8.7475	-5.8332
36	0.2852	-12.4349	-8.3064
37	0.2764	-9.8322	-6.5625
38	0.2712	-8.0342	-5.3586
39	0.2704	-9.3737	-6.2584
40	0.2600	-7.2324	-4.8230
41	0.2500	-9.4809	-6.3314
42	0.2400	-8.7247	-5.8244
43	0.2300	-8.8391	-5.9016
44	0.2100	-8.4974	-5.6732
45	0.1900	-8.2448	-5.5046
46	0.1700	-7.8063	-5.2116
47	0.1540	-6.9519	-4.6394
48	0.1470	-8.5951	-5.7428

49	0.1400	0.6263	0.4421
50	0.1340	-15.9913	-10.7001
51	0.1270	-9.1527	-6.1113
52	0.1200	-8.2461	-5.5041
53	0.1170	-7.9475	-5.3037
54	0.1150	-8.1710	-5.4520
55	0.1120	-9.0493	-6.0376
56	0.1120	-11.6936	-7.8057
57	0.1100	-22.7031	-15.1908

FIGURE CAPTIONS

1. Broadening coefficient, γ, vs. rotational quantum number J. Various symbols denoted in Figure legend represent different K values. The solid curve shows the scaling law fit with "unrestricted" collisional selection rules ($A^{\pm} \leftrightarrow A^{\pm}$ and $A^{+} \leftrightarrow A^{-}$). The scaling law curve obtained with "restricted" collisional selection rules ($A^{\pm} \leftrightarrow A^{\pm}$) is not distinguishable from the curve shown.

2. The $^{R}Q(J,8)$ Q branch of the ν_5 band. (a) shows the experimental transmission spectrum as a continuous curve and the computed spectrum as filled circles. The computed spectrum assumes overlapping Voigt spectral profiles and the line-intensity and frequency parameters discussed in this paper. The CH_3Cl pressure was 13.74 torr and absorbing path length 25 cm. The good agreement between the calculated and measured spectrum is shown in panel (b) as obs - calc, with scale shown on the right margin of the figure. This comparison shows that the spectral line parameters are good when lines in the Q branch do not strongly overlap.

3. The $^{R}Q(J,0)$ Q branch of the ν_5 band includes in a 0.1 cm^{-1} interval about fifty lines each for $CH_3{}^{35}Cl$ and $CH_3{}^{37}Cl$. The CH_3Cl pressure was 0.719 torr and absorbing path length 25 cm. (a) shows the experimental transmission spectrum as a continuous curve and the computed spectrum as filled circles. The computed spectrum assumes overlapping Voigt spectral profiles and the line-intensity and frequency parameters discussed in this paper. The water line at approximately 1459.26 cm^{-1} is fit as the superposition of a line at high and low pressures because of there was some water in the nominally evacuated FT vacuum chamber and a small ambient laboratory path. The discrepancy in trace (b) between obs-calc at the water line is due to a slightly incorrect position used for the water line.

4. Line mixing in the $^{R}Q(J,0)$ Q branch of the ν_5 band. (a) shows the experimental transmission spectrum as a continuous curve and the computed spectrum as filled circles. The CH_3Cl pressure was 13.74 torr and absorbing

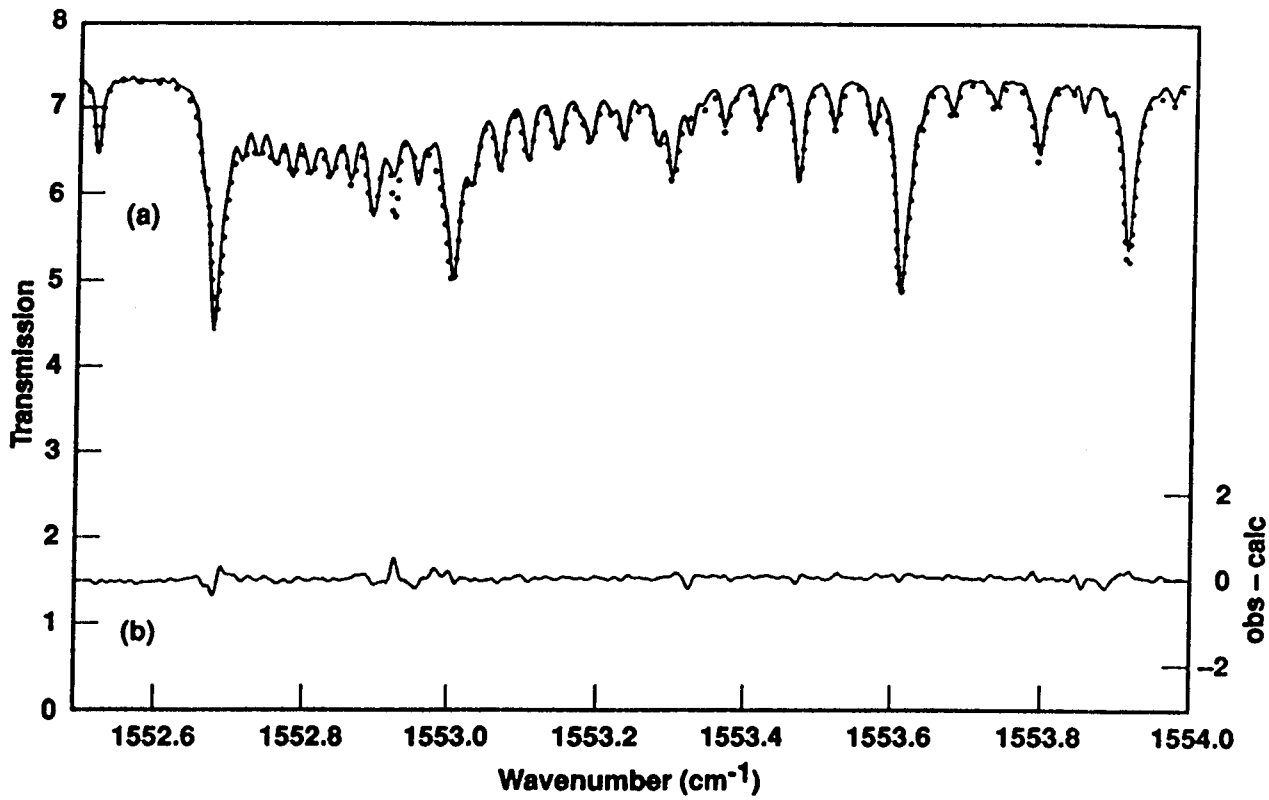
8
7
6
5
4
3
2
1
0
Transmission
(a)
(b)
2
0
−2
obs − calc
1552.6
1552.8
1553.0
1553.2
1553.4
1553.6
1553.8
1554.0
Wavenumber (cm-1)

Fig.

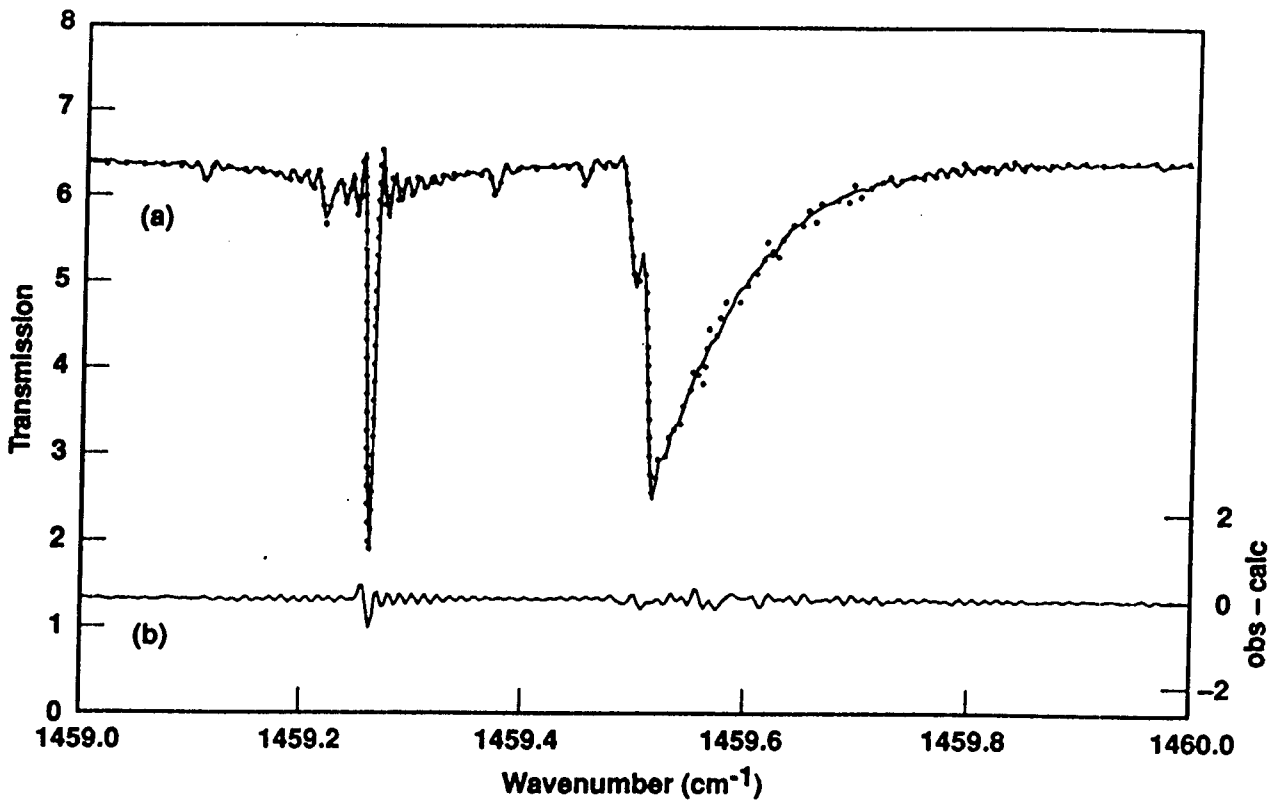
8
7
6
5
4
3
2
1
0
Transmission
(a)
(b)
2
0
−2
obs − calc
1459.0
1459.2
1459.4
1459.6
1459.8
1460.0
Wavenumber (cm-1)

Fig.

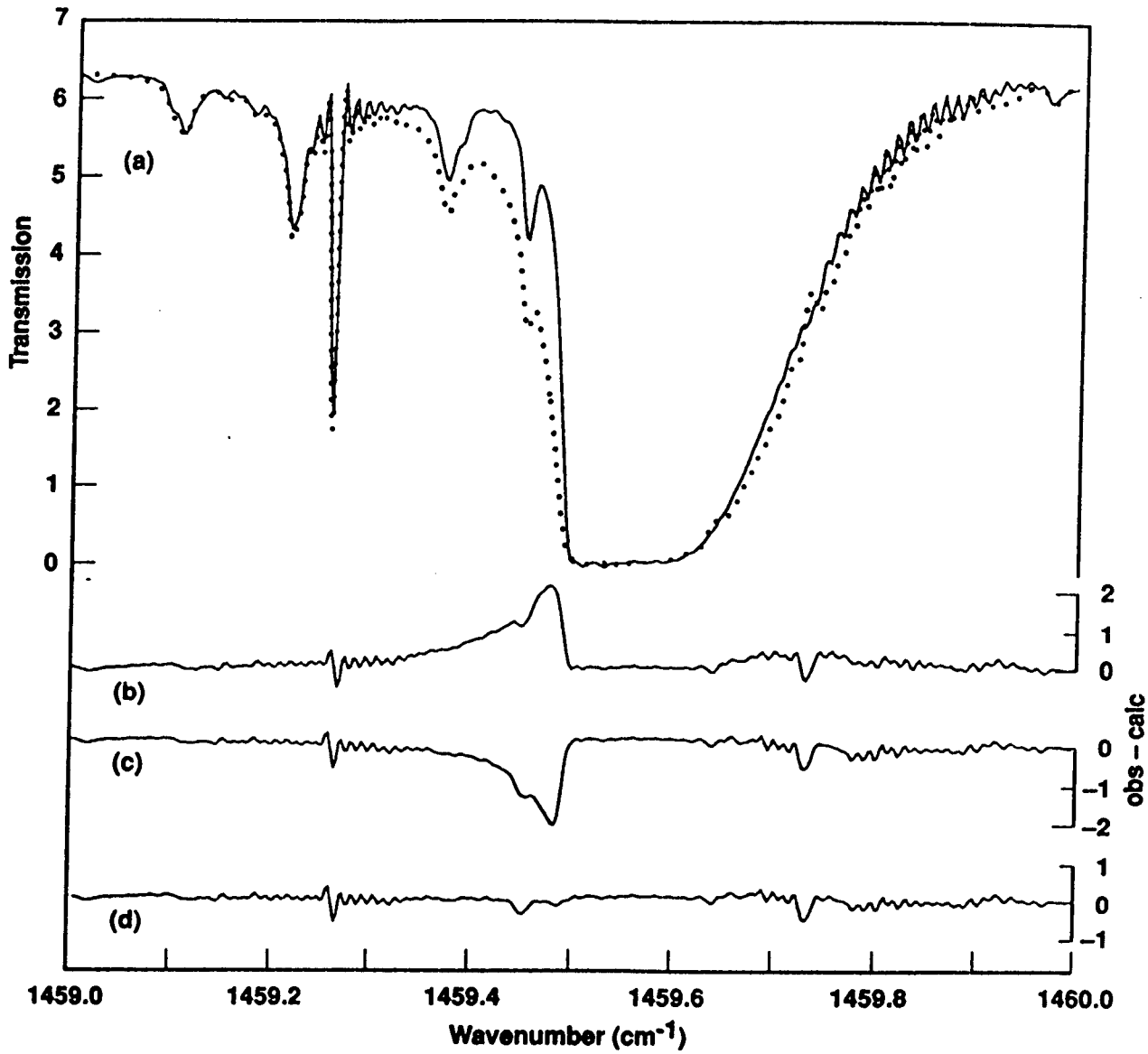
Transmission
7
6
5
4
3
2
1
0
(a)
(b)
(c)
(d)
2
1
0
0
−1
−2
1
0
−1
obs − calc
1459.0
1459.2
1459.4
1459.6
1459.8
1460.0
Wavenumber (cm^{-1})

Fig.

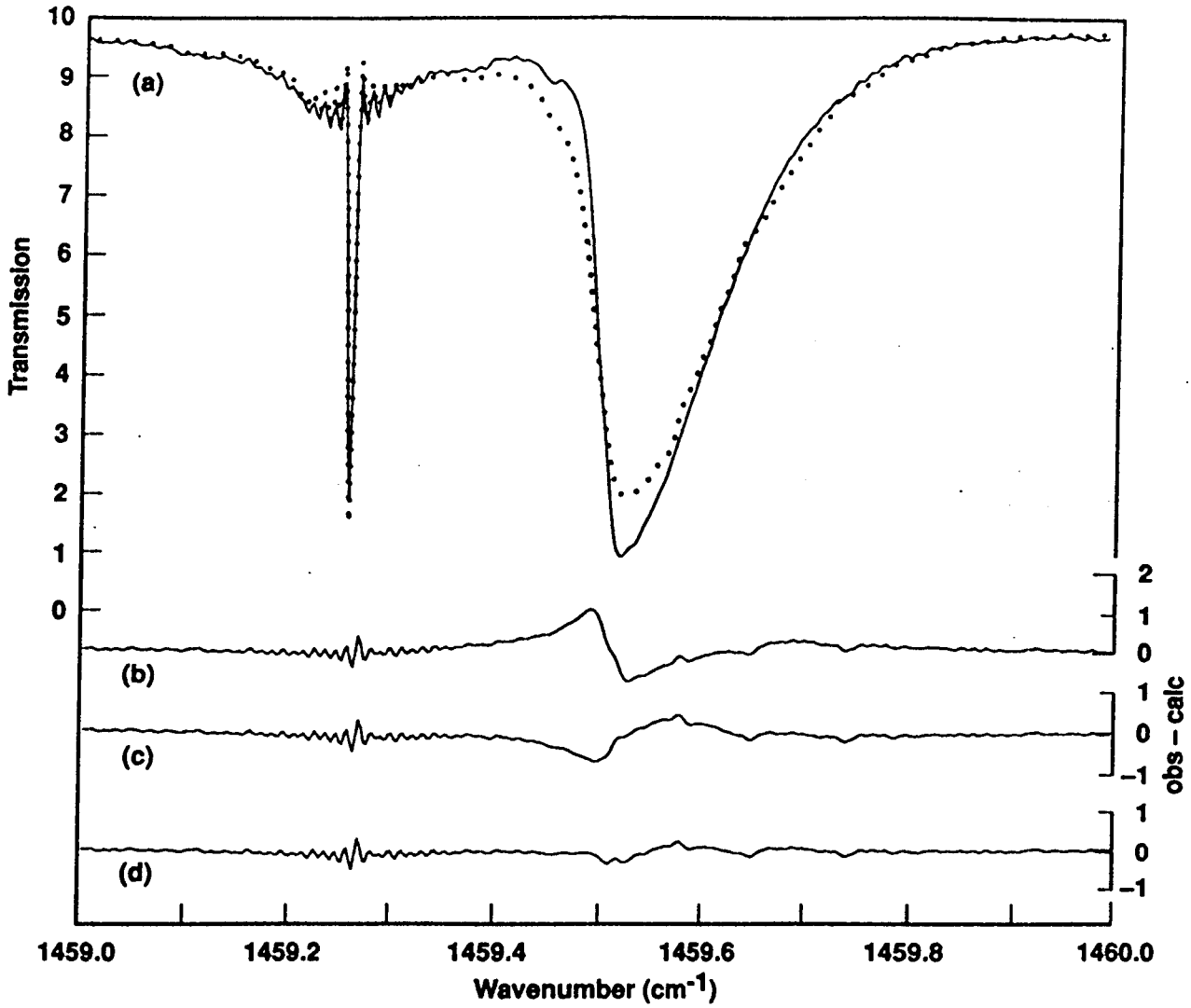
Transmission
10
9
8
7
6
5
4
3
2
1
0
(a)
(b)
(c)
(d)
2
1
0
1
0
−1
1
0
−1
obs − calc
1459.0
1459.2
1459.4
1459.6
1459.8
1460.0
Wavenumber (cm-1)

Fig.

path length 25 cm. The computed spectrum shown in (a) assumes overlapping Voigt spectral profiles. (b) shows the difference between the curves shown in (a). (c) shows the difference between the experimental and computed spectrum with line mixing included and $A^{\pm} \leftrightarrow A^{\pm}$ collisions allowed. (d) shows the difference between the experimental and computed spectrum with line mixing included and $A^{\pm} \leftrightarrow A^{\pm}$ and $A^{+} \leftrightarrow A^{-}$ collisions allowed.

5. The $^{R}Q(J,0)$ Q branch of the ν_5 band. (a) shows the experimental transmission spectrum as a continuous curve and the computed spectrum as filled circles. The CH_3Cl pressure was 23 torr and absorbing path length 2.63cm. The computed spectrum shown in (a) assumes overlapping Voigt spectral profiles. (b) shows the difference between the curves shown in (a). (c) shows the difference between the experimental and computed spectrum with line mixing included and $A^{\pm} \leftrightarrow A^{\pm}$ collisions allowed. (d) shows the difference between the experimental and computed spectrum with line mixing included and $A^{\pm} \leftrightarrow A^{\pm}$ and $A^{+} \leftrightarrow A^{-}$ collisions allowed.

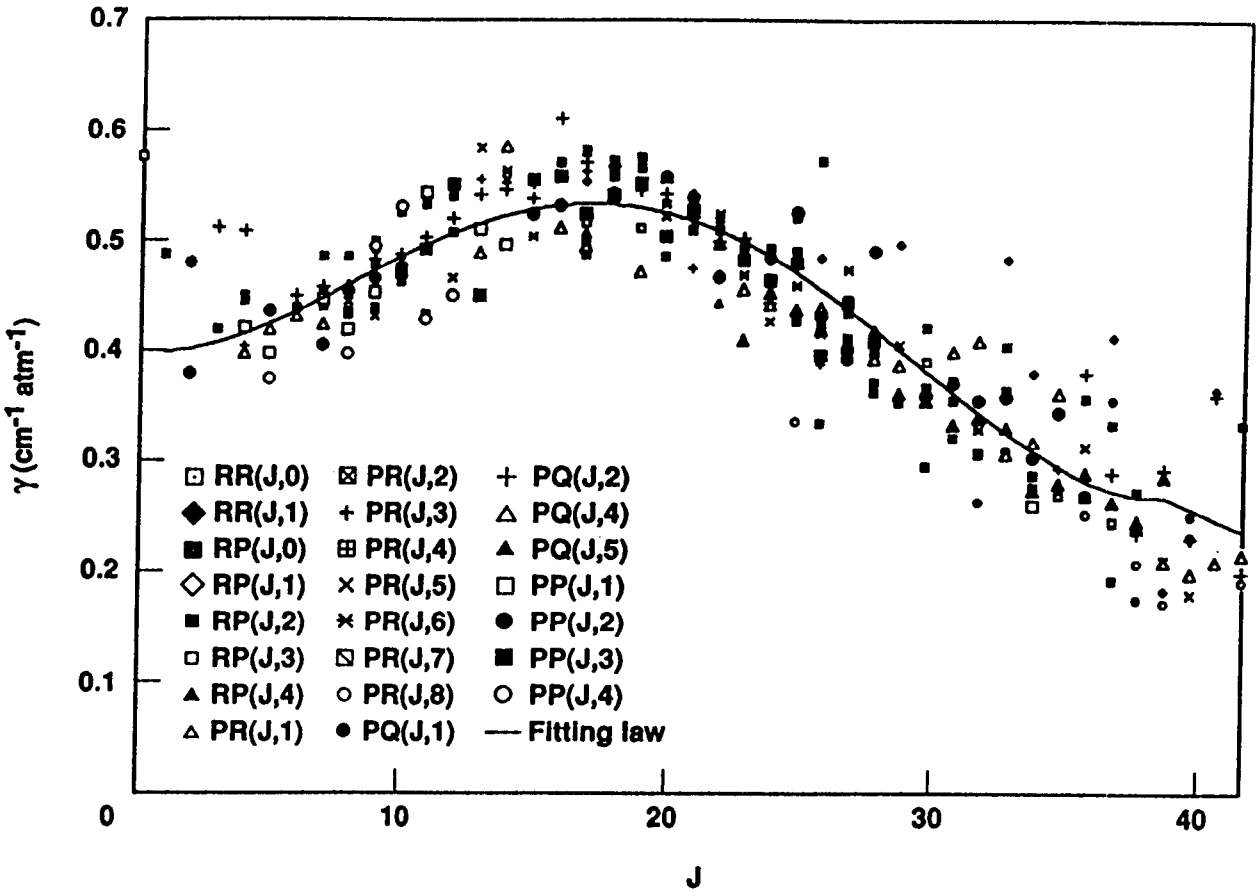
0.7
0.6
0.5
0.4
0.3
0.2
0.1
0
10
20
30
40
J
γ (cm⁻¹ atm⁻¹)
RR(J,0)
RR(J,1)
RP(J,0)
RP(J,1)
RP(J,2)
RP(J,3)
RP(J,4)
PR(J,1)
PR(J,2)
PR(J,3)
PR(J,4)
PR(J,5)
PR(J,6)
PR(J,7)
PR(J,8)
PQ(J,1)
PQ(J,2)
PQ(J,4)
PQ(J,5)
PP(J,1)
PP(J,2)
PP(J,3)
PP(J,4)
Fitting law

Fig.